Journal of Applied Fluid Mechanics, Vol. 11, No. 5, pp. 1287-1296, 2018.
Available online at www.jafmonline.net, ISSN 1735-3572, EISSN 1735-3645.
DOI: 10.29252/jafm.11.05.28668

Accuracy of Dynamic Stall Response for Wind Turbine Airfoils Based On Semi-Empirical and Numerical Methods

S. Rasekh†, M. Hosseini Doust and S. Karimian Aliabadi

Department of Aerospace Engineering, Tarbiat Modares University, Tehran, Iran

† *Corresponding Author Email: sepehrrasekh@modares.ac.ir*

(Received December 6, 2017; accepted February 17, 2018)

ABSTRACT

The aim of the present study is to investigate the accuracy of two different dynamic stall approaches for wind-turbine airfoils. The first approach is the semi-empirical Leishman-Beddoes model (L-B), and the second is the computational fluid dynamic (CFD) results. National Renewable-Energy Laboratory (NREL) S series airfoils are used, and the simulations are performed in $Re=10^6$. For both approaches, aerodynamic coefficients are represented and compared to experimental data. Validation data refer to Ohio State University (OSU) experiments, which are for pitch oscillation. Results show that the accuracy of the L-B and CFD methods is dependent on mean angle of attack, reduced frequency and the phase of motion. The semi-empirical model has appropriate accuracy as well as low computational cost while the CFD unsteady simulation could be properly used to predict the drag coefficient.

Keywords: Dynamic stall; Wind turbine airfoils; Semi-Empirical model; Numerical method.

1. INTRODUCTION

Dynamic stall has been shown to be an important phenomenon in wind-turbine blades, which will cause many destructive effects on the wind turbine performance and structure (Butterfield 1988). Presence of platform motions of offshore floating wind turbines, variation of pitch angle due to pitch control system and yaw/tilt misalignment are the most common reasons of dynamic stall occurrence (Liu, Yu *et al.* 2014). This phenomenon, dynamic stall, initiates with the formation of a vortex at the Leading Edge (LE) that sheds along the chord of the airfoil from LE to Trailing Edge (TE) (Leishman and Beddoes 1989). The vortex causes the maximum lift coefficient increases at dynamic stall situation, which is higher than the static case (Shipley, Miller *et al.* 1995). The increase of the maximum lift coefficient is due to the delay of stall occurrence and also the growth of circulation of the airfoil. As the vortex moves toward the TE, the center of pressure as well inclines to the TE. This movement will cause a nose-down torque which has some harmful effects on the wind turbine blades, because the distribution of this torque along the span is not uniform. Another effect of dynamic stall is the decrease of aerodynamic damping that boosts the possibility of occurrence of stall flutter (Gaertner and Lackner 2015).

The unsteady methods that can predict dynamic stall effects consist of experimental, computational fluid dynamics (CFD) and semi-empirical models. One of the most useful experimental data is the Ohio State University (OSU) experiment, which the effects of dynamic stall was investigated for some wind-turbine airfoils. Other experimental works that was carried out for S809 airfoil can be seen in Sheng, Galbraith *et al.* (2006) and Sheng, Galbraith *et al.* (2006). CFD also can represent dynamic stall physics and the consequences of this phenomenon on the aerodynamic properties of airfoils. With the improvement in numerical methods and turbulence modeling, the use of CFD is becoming increasingly possible. For instance, Gharali *et al.* (Gharali and Johnson 2012) simulated the dynamic stall behavior of S809 airfoil by a numerical method at erosion condition and high reduced frequencies. They have found that when the airfoil is at eroded condition, the lift decreases and causing an intensive outcome on wind turbine efficiency.

As mentioned before, another way to simulate the dynamic stall, is using Semi-Empirical models. These models can be applied in situations in which the CFD tools are not feasible to use. For this purpose, there are some common ways such as Leishman-Beddoes (Leishman and Beddoes 1989), Snel (Snel 1997), Gormont (Gormont 1973) and ONERA (Tran and Petot 1980) methods to imitate the effects of dynamic stall on aerodynamic force coefficients. L-B method has been used by many references (Elgammi & Sant 2016a, Elgammi & Sant 2016b). Gupta and Leishman

(Gupta & Leishman 2006) have proposed modified L-B method to model the dynamic stall of the S809 airfoil that is used in many wind-turbines, and they obtained good agreement between the predictions and experimental data. It was also shown that the hysteresis in the aerodynamic coefficients was captured well. They showed that the mathematical structure of the model is appropriate to be used for wind turbine applications.

Pereira *et al.* (Pereira, Schepers *et al.* 2013) have combined blade element theory with the L-B method and they have gotten proper results. In order to validate this combination, the experimental data of the MEXICO wind turbine was used. Holierhoek *et al.* (Holierhoek, De Vaal *et al.* 2013) have studied dynamic stall behavior of S809 airfoil with Semi-Empirical models. It was shown that there are still differences between measurements and models, especially when the airfoil experiences deep stall.

This investigation is formed to give an overview of the accuracy of the numerical simulation method using ANSYS Fluent 17 and a Semi-Empirical method in terms of the experimental data. The purpose is studying the effects of reduced frequency and mean angle of attack variations on the accuracy of dynamic stall models. The S825, S814 and S815 airfoils are used. Some properties of these airfoils are shown in Table1. The capabilities of these methods in upstroke and down stroke phases are investigated and compared to experimental data.

Table 1 Characteristics of studied airfoils (steady and clean airfoil)

	Thickness	Static Stall angle (deg.)	Max. lift coefficient
S825	0.17C	11.2	1.43
S814	0.24C	11	1.32
S815	0.26C	10-12	1.27

2. COMPUTATIONAL METHOD

Two-dimensional incompressible Unsteady Reynolds-Averaged Navier-Stokes (URANS) equations are employed for fluid flow simulations (Cai, Gu *et al.* 2016). All the simulations are conducted by the Commercial CFD solver ANSYS fluent 17. The equations of mass and momentum conservation that governing the fluid flow are as follows (Ebrahimi & Movahhedi 2017):

$$\frac{\partial \bar{u}_i}{\partial x_i} = 0 \tag{1}$$

$$\frac{\partial \bar{u}_i}{\partial t} + \bar{u}_j \frac{\partial \bar{u}_i}{\partial x_i} = -\frac{1}{\rho}\frac{\partial \bar{p}}{\partial x_i} + \nu \frac{\partial^2 \bar{u}_i}{\partial x_j \partial x_j} - \frac{\partial \overline{\acute{u}_i \acute{u}_j}}{\partial x_j} + G_i$$

In which $\overline{\acute{u}_i \acute{u}_j}$ is the well-known Reynolds stress tensor that should be calculated by turbulence models. $\bar{p}$, $\bar{u}$,G and ν are time-averaged static pressure, time-averaged velocity, body forces and kinematic viscosity, respectively.

2.1 Grid generation

As all the simulations are planar, the two-dimensional C-type mesh is used. In order to verify the independency of the numerical solution and results from the computational grid, a study was conducted using three computational grids with the different number of cells at steady condition with angle of attack of 3°. The results are shown in Table 2 for S825 airfoil. The results of the study reveal that the total number of 85000 cells is suitable for all the simulations. The structural mesh around airfoils was generated with 400 elements along the chord wise direction. The Full computational domain and near airfoil meshes are shown in Fig. 1. The effect of non-dimensional wall distance y^+ is also considered in a way that the first node is in the viscous sub layer region. Therefore, the parameter of y^+ on the airfoil surface is set to be less than one ($y^+<1$) to achieve acceptable results. Since the airfoil is oscillating about ¼ chord, the dynamic mesh method is employed. The so-called user-defined function (UDF) was also used to oscillate the airfoil about ¼ chord.

Table 2 Grid independency results

Parameters	Number of Cells		
	80000	85000	90000
C_l	0.885	0.901	0.906
C_d	0.0179	0.01803	0.01809

2.2 Boundary Conditions

Pressure far-field boundary condition is applied to the boundaries which are far enough from airfoil at about distance of 20C that simulate the wind tunnel flow conditions (C is the airfoil chord length). On the airfoil surface, the no slip condition is defined. At the inlet boundary, an axial flow is specified with a velocity and pressure equal to atmospheric pressure.

2.3 Simulation Properties

As flow is fully turbulent, thus the shear-stress transport (SST) k−ω which is a combination of k-ω and k-ε models is applied to the URANS model in order to capture the turbulence flow effects (Menter 1994, Menter, Kuntz *et al.* 2003). The SST k−ω model is capable of capturing the flow structures of dynamic airfoils associated with LEV formations for a wide range of Reynolds numbers with an acceptable accuracy (Rival, Hass *et al.* 2011). Pressure-based solver has been employed to solve the equations of mass and momentum. The pressure-velocity coupling is set to PISO algorithm and second order upwind scheme is chosen for spatial discretization. Acceptable residual criterion in magnitude is in order of 10^{-6}. Characteristic time for airfoil is $t_f = \frac{C}{U}$ and the time step size is chosen in such a way that satisfies t_f and even 10^2 times smaller the time step size is used. Therefore, the average time step is equal to 10^{-4} second. The CPU cost for every cycle took about two days using six CPUs parallel processing.

3. LEISHMAN-BEDDOES METHOD

This method is performed by three stages. First, the unsteady attached inviscid flow results are calculated

then the effect of separation is added and finally the effect of Leading Edge Vortex(LEV) will be calculated in order to capture the dynamic stall effects(Leishman and Beddoes 1989, Gupta and Leishman 2006).

3.1 Unsteady Attached Flow

Firstly, a model should be proposed that can predict attached flow behavior of the airfoil. By using indicial response method, this prediction will be done. In indicial response method, the assumption is that the flow is fully attached even at post stall condition. In this method, the solution consists of two parts. The first part is the circular part of loads, and the second part is non-circular or added mass loading.

It should be noted that the following equations consist of the circulatory part with superscript of (c), and the non-circulatory part with superscript of (nc) and the pitching

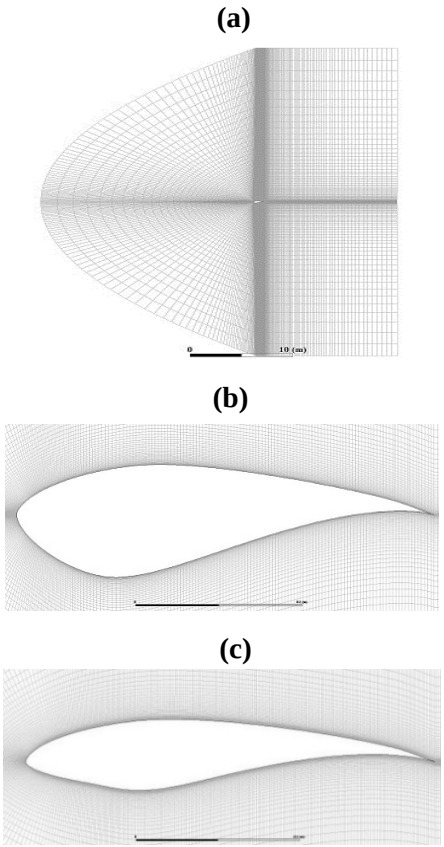

Fig. 1. (a) Full computational domain. (b) Details of mesh around S815 airfoil. (c) Details of mesh around S825 airfoil.

rate is defined as $q = \frac{\alpha c}{U}$. All the coefficients have been used in the L-B method are given in table 3. The total circular part of the normal force can be expressed(Gupta and Leishman 2006) as:

$$C_n^c = C_{n_\alpha} \alpha_e(s, M) \tag{2}$$

In Eq. (2) equivalent angle of attack $\alpha_e(s, M)$ is defined(Gupta and Leishman 2006) as:

$$\alpha_e(s, M) = \alpha - X(s) - Y(s) \tag{3}$$

In Eq. (3) the $X(s)$ and $Y(s)$ can be expressed(Gupta and Leishman 2006) as:

$$X(s) = X(s - \Delta s)\exp(-b_1\beta^2\Delta s) + A_1\Delta\alpha\exp\left(-\frac{b_1\beta^2\Delta s}{2}\right) \tag{4}$$

$$Y(s) = Y(s - \Delta s)\exp(-b_2\beta^2\Delta s) + A_2\Delta\alpha\exp\left(-\frac{b_2\beta^2\Delta s}{2}\right) \tag{5}$$

In the above equations, M is Mach number, S is non-dimensional time and $\beta = \sqrt{1 - M^2}$. In order to calculate the non-circulatory (C_n^{nc}) part of the normal force, the reference (Hansen, Gaunaa *et al*. 2004) can be used.

3.2 Unsteady Separated Flow

Secondly, the effect of separation from leading edge should also be accounted. For this purpose, the Kirchhoff(Thwaites and Street 1960) theory which provide the relation between normal force coefficient C_n and separation point f (where f is the location of the flow separation point non-dimensioned by the chord length) can be expressed as:

$$C_n^f = C_{n_\alpha}\left(\frac{1+\sqrt{f}}{2}\right)^2 \sin(\alpha - a_0) \tag{6}$$

Where a_0 is zero lift angle of attack. Equation (6) is suitable for steady state condition. In order to use it at unsteady conditions, the f should be modified by adding leading edge pressure distribution and unsteady boundary layer response effects(Leishman and Beddoes 1989). Then, considering the leading edge pressure distribution, the normal force lag equation can be defined as:

$$C'_{n_k} = C_{n_k}^{pot} - D_{p_k} \tag{7}$$

Where D_{p_n} can be written as:

$$D_{p_k} = D_{p_{k-1}}\exp\left(-\frac{\Delta s}{T_p}\right) + (C_{n_k}^{pot} - C_{n_{k-1}}^{pot})\exp\left(-\frac{\Delta s}{2T_p}\right) \tag{8}$$

According to new normal force C'_{n_n}, modified angle of attack will be expressed as:

$$\alpha_f(t) = \frac{C'_{n_k}}{C_{n_\alpha}} + a_0 \tag{9}$$

By substituting Eq. (9) to (6), effective separation point $\acute{f}$ will be calculated. The additional effect that should be considered is the unsteady boundary layer response, to considering it, $\ddot{f}$ will be expressed as:

$$\ddot{f} = \acute{f} - D_{f_k} \tag{10}$$

Where:

$$D_{f_k} = D_{f_{k-1}}\exp\left(-\frac{\Delta s}{T_f}\right) + (f_k - f'_{k-1})\exp\left(-\frac{\Delta s}{2T_f}\right) \tag{11}$$

Then the normal force coefficient can be expressed as:

$$C_n^f = C_{n_\alpha}\left(\frac{1+\sqrt{f}}{2}\right)^2 \sin(\alpha_e - \alpha_0) \quad (12)$$

The chord wise force coefficient also can be written by using Kirchhoff theory (Leishman and Beddoes 1989) as:

$$C_a = C_{n_\alpha}\sqrt{f}\,(\alpha - \alpha_0)\sin(\alpha - \alpha_0) \quad (13)$$

3.3 Vortex Lift Effects

To consider the effects of LEV formation, the normal force due to the vortex shedding $C_{n_k}^v$ can be calculated (Leishman and Beddoes 1989) by:

$$C_{n_k}^v = C_{n_{k-1}}^v \exp\left(-\frac{\Delta s}{T_v}\right) + (C_{v_k} - C_{v_{k-1}})\exp\left(-\frac{\Delta s}{2T_v}\right) \quad (14)$$

Where:

$$C_{v_k} = C_{n_k}^c(1 - K_n)\,; \quad K_n = \left(\frac{1+\sqrt{f}}{2}\right)^2 \quad (15)$$

Finally, by summing the results of Eqs. (12) and (14) with non-circulatory part of the normal force (C_n^{nc}), the total normal force coefficient under dynamic stall can be expressed(Gupta and Leishman 2006) as Eq. (16):

$$C_n = C_n^v + C_n^f + C_n^{nc} \quad (16)$$

Table 3 Coefficients and constants of L-B method (Gupta and Leishman 2006)

A1	A2	B1	B2
0.3	0.7	0.14	0.53
T_v	T_f	T_p	
1.7	3.0	6.0	

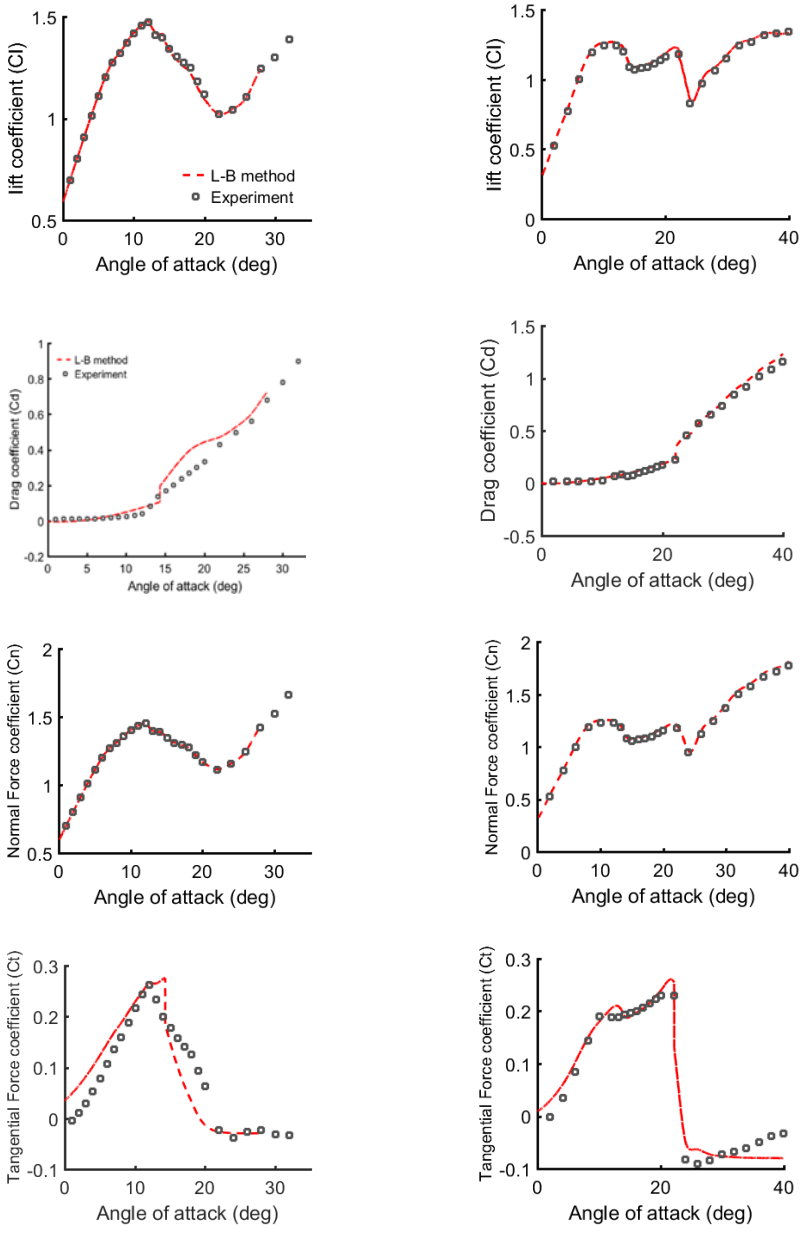

(a) **(b)**

Fig. 2. Comparison between experimental data and L-B method at steady condition for a) S825 b) S815.

3.4 L-B Results At Steady Condition

In this method, the static results should also be represented, because the proper representation of the static characteristics is very important for the success of the L–B model. For this sake, the steady results of the OSU experiment are being compared with the results of L-B method at k~0. The results are shown in Fig. 2. As it is clear, good agreement was obtained with the experimental data.

The relation between f and the angle of attack(deg) for each airfoil is represented by a polynomial equation as:

$$f(\alpha) = B_0 + B_1\alpha^1 + B_2\alpha^2 + \cdots + B_7\alpha^7 \quad (17)$$

The relation was gained by curve fitting of the experimental data at steady condition. The value of the $B_0 - B_7$ are shown in table 4.

4. EXPERIMENTAL DATA

As mentioned before, the experimental data of OSU measurement are used as the basis of comparison of the models. In OSU measurements, the unsteady pitching motion of some wind turbine airfoils is being examined under range of reduced frequencies, mean angles of attack and oscillating amplitudes at $Re>0.75\times10^6$(Janiszewska, Ramsay *et al*. 1996, Reuss Ramsay, Hoffman *et al*. 1996, Ramsay 1998). Reynolds number, Re, is defined as $Re = \frac{\rho U c}{\mu}$, in which U, c, ρ and μ are free-stream velocity, chord length, flow density and dynamic viscosity, respectively. It should be mentioned that the drag coefficient from the OSU data is based on the wake drag coefficient and friction drag is not considered.

5. COMPARISON TO UNSTEADY DATA

The first method of comparing the results is to plot figures displaying both the measured and modelled aerodynamic coefficients polar. To enable a comparison between different models, the error function can be used to give an explanation of the difference between the measured and calculated outcomes. This function can be represented as:

$$error = C_{l,model} - C_{l,exp}$$

or

$$error = C_{d,model} - C_{d,exp} \quad (18)$$

Table 4 Coefficients of Eq. (17) at $Re=10^6$

	S825 airfoil	S815 airfoil	S814 airfoil
B_0	1.006	0.9166	0.9511
B_1	0.000102	0.01615	0.00586
B_2	0.005037	0.0202	-0.0465
B_3	-0.00158	-0.005336	0.01658
B_4	0.0001	0.000433	-0.00257
B_5	-3.03×10^{-6}	-1.625×10^{-5}	0.00018
B_6	3.37×10^{-8}	2.918×10^{-7}	-5.155×10^{-6}
B_7	-8.52×10^{-11}	-2.03×10^{-9}	7.11×10^{-8}

The overall error E_T is defined to help deciding which method is more accurate than the other one at up stroke, down stroke phases and also for a complete cycle as:

$$E_T = \frac{\sum_1^N (error)_i^2}{N} \quad (19)$$

In which N is the number of error vector components that can be changed by increasing or decreasing the time interval in the calculations.

In wind turbine applications, the maximum lift coefficient is very important since if the lift force exceeds a specific value, the structure will fail. Therefore, it is important that the models predict the maximum lift coefficient as accurate as possible. For this purpose, the highest lift coefficient prediction of both methods is being compared with measured data.

6. RESULTS AND DISCUSSION

In this section the results of unsteady pitching motion of the mentioned airfoils are presented and the effects of mean angle variation and reduced frequency variation on the accuracy of all the methods are investigated. The pitching motion of all the airfoils is defined as the following equation:

$$\alpha(t) = \alpha_{mean} + \alpha_{amp}\sin(\omega t) \quad (20)$$

Where ω is the frequency of oscillation in (rad/s) and can be expressed as:

$$\omega = \frac{kU}{b} \quad (21)$$

In which b and k are semi-chord length and reduced frequency of oscillation respectively. It should be noted that the lift coefficient is defined as $C_l = \frac{L}{0.5\rho U^2 c}$ where L is lift force and drag coefficient is defined as $C_d = \frac{D}{0.5\rho U^2 c}$ where D is drag force.

6.1 Effects of Reduced Frequency

The purpose of this section is to investigate the effects of reduced frequency variations on the accuracy of CFD and L-B methods. For this sake, the accuracy of the dynamic stall models is investigated for S814 airfoil at mean angle of attack 8°, oscillating amplitude of 10°, and the reduced frequencies of 0.03 and 0.089. Figure 3 shows the results of the simulations at k=0.03 and k=0.089 for both methods. Results of the Table 5 show that the accuracy of the methods to predict the lift coefficient at upstroke phase is better at higher reduced frequencies. However, at down stroke phase the increase of reduced frequency, decreases the accuracy of the methods. The comparison of the results of L-B method with CFD results indicates that the L-B method is usually more accurate than the CFD results at both phases. For instance, the total error of the L-B method at upstroke phase is less than one percent, but error at the same phase for CFD is about 3 percent. The results of the drag coefficient show that the CFD is more accurate than the L-B method. It can be seen that increase of the reduced frequency decreases the accuracy of both the methods.

Results of unsteady models show that as the reduced

frequency increases, the maximum lift coefficient also growths. The reason is that the angle of attack where the stall happens also rises. For instance, at k=0.03, the stall happens at angle of attack of 14º, but at the higher reduced frequency the stall angle of attack rises to 16.5º. These effects also are captured well with both methods. The maximum lift coefficient that each method predicts and the percentage of relative error of each method respect to experimental data are shown in Table 6. There is an acceptable agreement between methods and experimental data. At reduced frequency of 0.03 the methods overestimate the maximum lift coefficient, but at higher reduced frequency the methods underestimate the maximum lift coefficient.

6.2 Effects of Mean Angle Of Attack

In this part, the effect of mean angle variation on the accuracy of the methods is investigated. For this purpose, the S825 and S815 airfoils are chosen. The simulations for both the airfoils were performed at two conditions. Firstly, the simulations are carried out at the reduced frequency of 0.08, the amplitude angle of 10º and mean angle of attack 8º. Then, the mean angle of attack increases to 14º. In Figs. 4 and 5 the unsteady lift drag coefficients of both the airfoils are represented at the mean angle of 8º and 14º.The results show that in all cases, when the airfoil experiences the upstroke motion, the change of lift coefficient with angle of attack is linear until the flow separated and stall happened. The maximum lift coefficient also increases due to the delay of stall occurrence. For instance, in case of S825 airfoil, the maximum lift coefficient increases from 1.43 at steady condition to 2. The increase of maximum lift coefficient angle of attack also can be seen from results of the models. Therefore, both the methods can predict the unsteady effects of dynamic stall. Table. 7 indicates that there is agreement between experimental maximum lift coefficient and the prediction of the methods, and the effect of mean angle growth on the accuracy of the methods is not tangible. Experimentally, in case of $\alpha_{mean} = 8^{o}$ the maximum lift coefficient occurs at angle of attack of 16.1º. The L-B method predicts the angle of attack of 16.2º, and the CFD method predicts angle of attack of 17.09º. It can be concluded that L-B method is more accurate than the CFD in case of forecasting the maximum lift coefficient angle of attack.

It can be inferred from Tables 8 and 9, the increase of mean angle of attack will usually increase the error of the models for both airfoils. It can also be seen that the accuracy of the L-B method is more than the CFD, especially at up stroke stage.

It should be mentioned that at the up stroke phase, the leading edge vortex (LEV) is dominant and should be taken into consideration. However, at the down stroke phase the trailing edge vortex (TEV) plays a prominent role. So the interaction of this vortex with LEV makes the flow complex (Gharali and Johnson 2012). Therefore, considering this interaction is very difficult and the CFD method cannot capture this interaction completely. These interactions can be seen from Fig. 6, which the vorticity contours of the flow around airfoil at mean angle of 14º is represented for S815 airfoil. It is obvious that at down stroke stage, the interaction of LEV and TEV plays a prominent role. This interaction may be captured better if other turbulence models like DNS and LES will be implemented in simulations.

The low accuracy of L-B method at down stroke stage also indicates that the method should be changed in a way that the effect of these interactions adds to the method. Moreover, improving the L-B method to capture the dynamic stall influences at high angle of attack will boost the accuracy of the L-B method. It can be also inferred that the fluctuations of lift coefficient that are shown in Fig. 5 is because of the effect of eddies that is represented in down stroke stage, especially when the flow is not fully reattached.

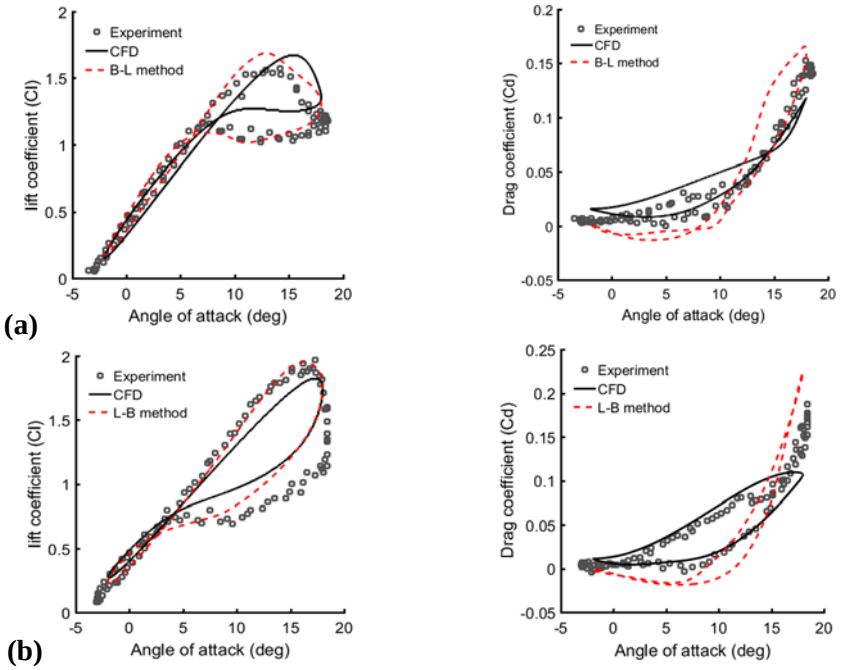

Fig. 3. Comparison between the experimental data, CFD and L-B method for S814 a) k=0.03 and b) k=0.089.

Table 5 Overall error of C_l and C_d for s814 airfoil at different reduced frequencies

	Lift coefficient				Drag coefficient			
K	Up stroke CFD	Down stroke CFD	Up stroke L-B	Down stroke L-B	Up stroke CFD	Down stroke CFD	Up stroke L-B	Down stroke L-B
0.03	0.0246	0.0209	0.0099	0.0027	0.00028	0.00005	0.0007	0.00014
0.089	0.0069	0.0424	0.0014	0.0458	0.0004	0.0002	0.0020	0.0012

Table 6 Maximum lift coefficient and percentage of relative error for s814 airfoil

	$C_{l,max}$			Relative Error(%)	
K	L-B	CFD	Exp.	L-B	CFD
0.03	1.69	1.67	1.57	7.64	6.36
0.089	1.95	1.82	1.97	1.01	7.61

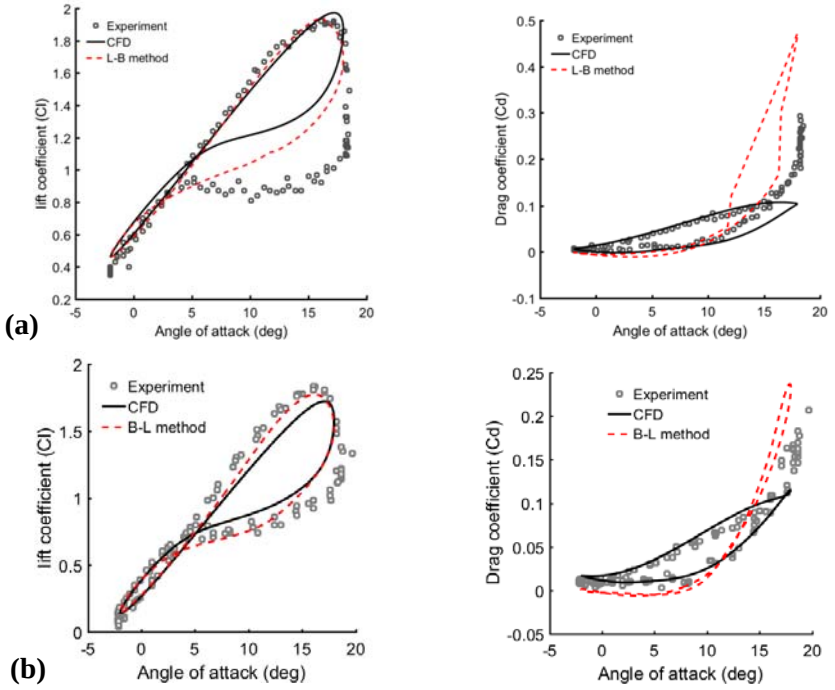

Fig. 4. Comparison of experimental data with CFD and L-B methods at k=0.08, α_{amp}=10°, α_{mean}=8° for a) S825 b) S815 airfoils.

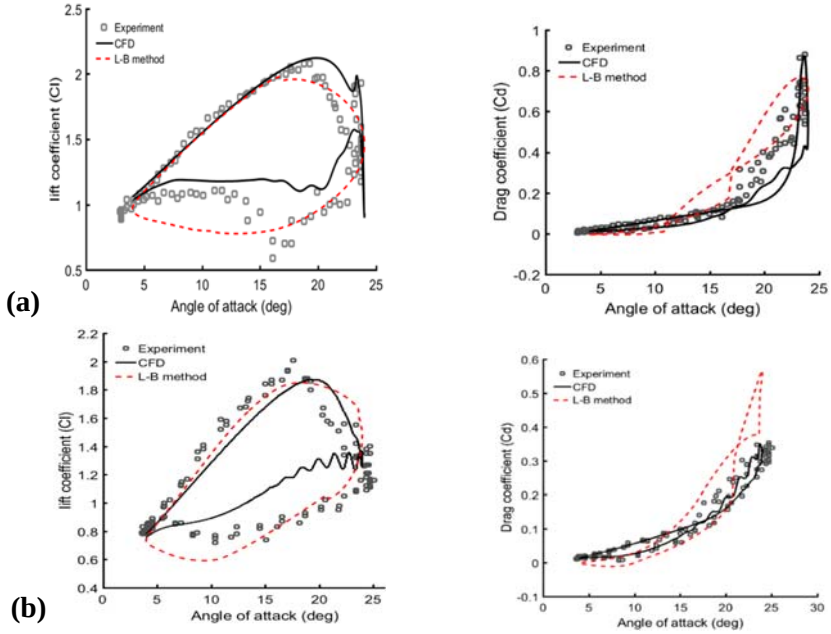

Fig. 5. Comparison of L-B and CFD methods with measurement at k=0.08, α_{amp}=10°, α_{mean}=14° for a) S825 b) S815 airfoils.

Table 7 Maximum lift coefficient and percentage of relative error for s825 and s815 airfoils at different mean angles of attack

	S825 airfoil					S815 airfoil				
	$C_{l,max}$			Relative Error(%)		$C_{l,max}$			Relative Error(%)	
Mean (deg.)	L-B	CFD	Exp.	L-B	CFD	L-B	CFD	Exp.	L-B	CFD
8	1.94	1.97	1.92	1.04	2.6	1.83	1.72	1.83	0	6.01
14	1.98	2.12	2.08	4.8	1.92	1.85	1.87	2.01	7.96	6.96

Table 8 Overall error of C_l and C_d for s825 airfoil at different mean angles of attack

	Lift coefficient				Drag coefficient			
Mean (deg.)	Up stroke CFD	Down stroke CFD	Up stroke L-B	Down stroke L-B	Up stroke CFD	Down stroke CFD	Up stroke L-B	Down stroke L-B
8	0.0058	0.1186	0.0020	0.0557	0.0011	0.0015	0.0112	0.0194
14	0.0147	0.0543	0.0082	0.0278	0.0110	0.0078	0.0141	0.0043

Table 9 Overall error of C_l and C_d for s815 airfoil at different mean angles of attack

	Lift coefficient				Drag coefficient			
Mean (deg.)	Up stroke CFD	Down stroke CFD	Up stroke L-B	Down stroke L-B	Up stroke CFD	Down stroke CFD	Up stroke L-B	Down stroke L-B
8	0.0118	0.0229	0.0025	0.0219	0.00039	0.00004	0.0015	0.00068
14	0.0144	0.0327	0.0167	0.0245	0.0013	0.00087	0.0065	0.0157

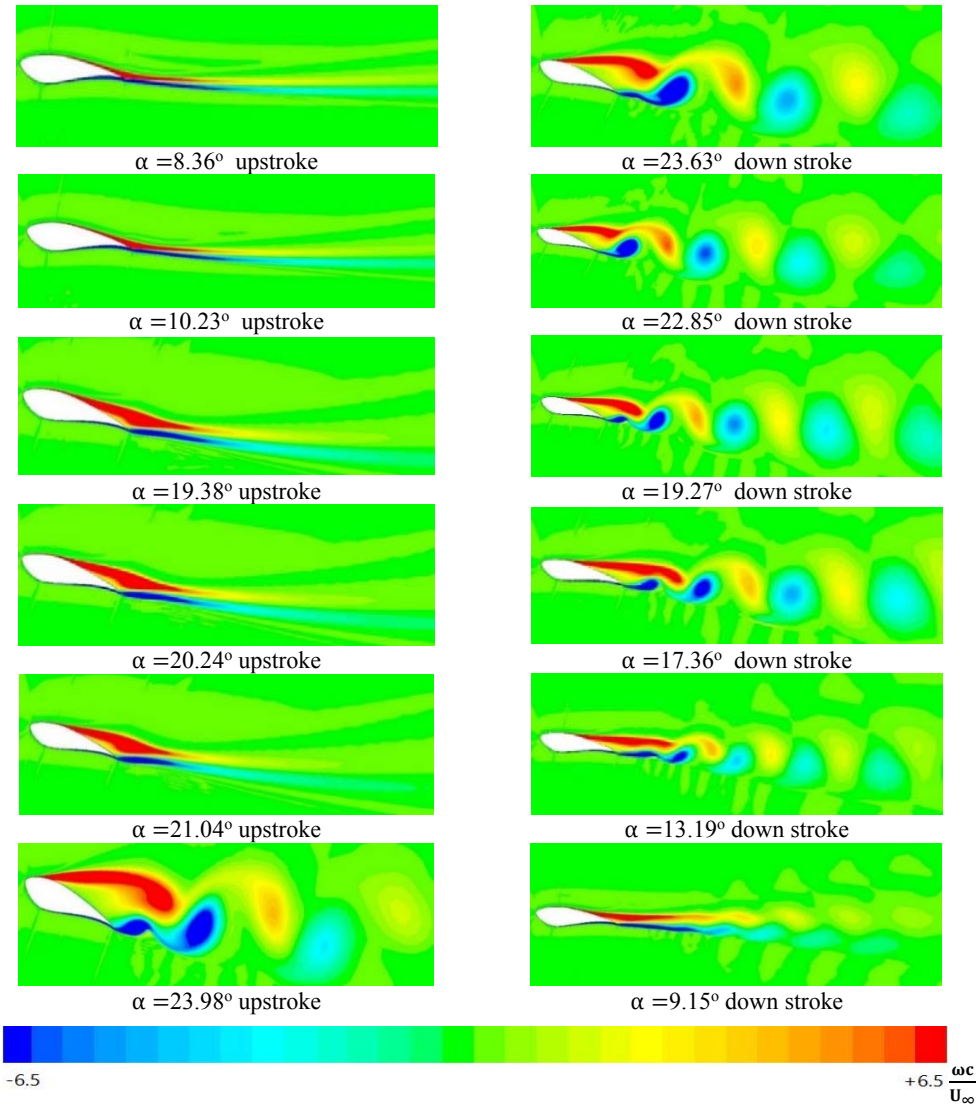

Fig. 6. Vorticity contours of S815 airfoil at k=0.08 and $\alpha_{mean} = 14^o$.

7. CONCLUSION

In this research two different approaches for prediction of dynamic stall in several thick airfoils which are almost used in the wind turbine blades are being examined based on the valid experimental data. One may think of the level of accuracy for both semi-empirical and CFD analysis methods and knowing the suitable condition for each method to be used. For the comparison, the force coefficients of OSU experiment are used. The main findings of the present study can be summarized as follows:

- The parametric study to investigate the effects of the mean angle of attack variations leads us to conclude that growth of mean angle of attack will decrease the accuracy of the L-B and CFD methods. Other important item to be pointed is the better prediction of both methods in upstroke while the lack of accuracy in down stroke is being deduced.
- The parametric study also indicates that the accuracy of the methods is dependent on the reduced frequency and the phase of the motion. It can be seen that at upstroke phase, both methods are more precise at high reduced frequencies. However, at down stroke phase, the methods are more precise at low reduced frequencies.
- The accuracy of the methods to predict the maximum lift coefficient is independent of reduced frequency and mean angle of attack. Both methods have the ability to predict the maximum lift coefficient precisely.
- The CFD's ability to capture the unsteady behavior of the dynamic stall phenomenon such as fluctuations of the lift coefficient is better than the L-B method especially at deep stall condition. However, the effects of LEV and TEV interaction that affects the accuracy of the CFD method at down stroke phase cannot be captured well. One good suggestion for continuing this work is developing the existed semi-empirical method to include such interactions. Furthermore, the effect of other turbulence models such as LES and DNS on the accuracy of dynamic stall modeling should be investigated in future. The CFD results can be noticed where the high accuracy drag estimation in transient manner is demanded.

REFERENCES

Butterfield, C. P. (1988). *Aerodynamic pressure and flow-visualization measurement from a rotating windturbine blade*, Solar Energy Research Inst., Golden, CO (USA).

Cai, X., R. Gu, P. Pan and J. Zhu (2016). Unsteady aerodynamics simulation of a full-scale horizontal axis wind turbine using CFD methodology. *Energy Conversion and Management 112*. 146-156.

Ebrahimi, A. and M. Movahhedi (2017). Power improvement of NREL 5-MW wind turbine using multi-DBD plasma actuators. *Energy Conversion and Management 146*. 96-106.

Elgammi, M. and T. Sant (2016a). Integrating a new flow separation model and the effects of the vortex shedding for improved dynamic stall predictions using the Beddoes–Leishman method. *Wind Energy 19*(11). 2089-2112.

Elgammi, M. and T. Sant (2016b). A Modified Beddoes–Leishman Model for Unsteady Aerodynamic Blade Load Computations on Wind Turbine Blades. *Journal of Solar Energy Engineering 138*(5). 051009.

Gaertner, E. M. and M. A. Lackner (2015). Modeling dynamic stall for a free vortex wake model. *Wind Engineering 39*(6). 675-691.

Gharali, K. and D. A. Johnson (2012). Numerical modeling of an S809 airfoil under dynamic stall, erosion and high reduced frequencies. *Applied Energy 93*. 45-52.

Gormont, R. E. (1973). *A mathematical model of unsteady aerodynamics and radial flow for application to helicopter rotors*, Boeing Vertol Co Philadelphia Pa.

Gupta, S. and J. G. Leishman (2006). Dynamic stall modelling of the S809 aerofoil and comparison with experiments. *Wind Energy 9*(6). 521-547.

Hansen, M. H., M. Gaunaa and H. A. Madsen (2004). *A Beddoes-Leishman type dynamic stall model in state-space and indicial formulation*s.

Holierhoek, J., J. De Vaal, A. Van Zuijlen and H. Bijl (2013). Comparing different dynamic stall models. *Wind Energy 16*(1). 139-158.

Janiszewska, J., R. R. Ramsay, M. Hoffmann and G. Gregorek (1996). *Effects of grit roughness and pitch oscillations on the S814 airfoil*, National Renewable Energy Lab., Golden, CO (United States).

Leishman, J. G. and T. Beddoes (1989). A Semi-Empirical Model for Dynamic Stall. *Journal of the American Helicopter society 34*(3). 3-17.

Liu, P., G. Yu, X. Zhu and Z. Du (2014). Unsteady aerodynamic prediction for dynamic stall of wind turbine airfoils with the reduced order modeling. *Renewable Energy 69*. 402-409.

Menter, F., M. Kuntz and R. Langtry (2003). Ten years of industrial experience with the SST turbulence model. Turbulence, *Heat And Mass Transfer 4*(1). 625-632.

Menter, F. R. (1994). Two-equation eddy-viscosity turbulence models for engineering applications. *AIAA Journal 32*(8). 1598-1605.

Pereira, R., G. Schepers and M. D. Pavel (2013). Validation of the Beddoes–Leishman dynamic stall model for horizontal axis wind turbines using MEXICO data. *Wind Energy 16*(2). 207-219.

Ramsay, R. R., Hoffmann, M. J., and Gregorek, G. M., (1998). *Effects of Grit Roughness and Pitch Oscillations on the S825 Airfoil*. National

Renewable Energy Lab., Golden, CO (United States); Ohio State Univ., Columbus, OH (United States).

Reuss Ramsay, R., M. Hoffman and G. Gregorek (1996). *Effects of grit roughness and pitch oscillations on the S815 airfoil*, National Renewable Energy Lab., Golden, CO (United States); Ohio State Univ., Columbus, OH (United States).

Rival, D., G. Hass and C. Tropea (2011). Recovery of energy from leading-and trailing-edge vortices in tandem-airfoil configurations. *Journal of Aircraft 48*(1): 203-211.

Sheng, W., R. Galbraith, F. Coton and R. Gilmour (2006). The collected data for tests on an S809 airfoil, volume I: pressure data from static, ramp and triangular wave tests. GU Aero Report 606.

Sheng, W., R. Galbraith, F. Coton and R. Gilmour (2006). The collected data for tests on an S809 airfoil, volume II: pressure data from static and oscillatory tests. GU Aero Report 607.

Shipley, D. E., M. S. Miller and M. C. Robinson (1995). *Dynamic stall occurrence on a horizontal axis wind turbine blade*, National Renewable Energy Lab., Golden, CO (United States).

Snel, H. (1997). *Heuristic modelling of dynamic stall characteristics.* Ewe Cconference Book Shop For Scientific Publications.

Thwaites, B. and R. Street (1960). Incompressible aerodynamics. *Physics Today 13*. 60.

Tran, C. and D. Petot (1980). Semi-empirical model for the dynamic stall of airfoils in view of the application to the calculation of responses of a helicopter blade in forward flight.